JACS
JOURNAL OF THE AMERICAN CHEMICAL SOCIETY
Article
pubs.acs.org/JACS

$Au_{99}(SPh)_{42}$ Nanomolecules: Aromatic Thiolate Ligand Induced Conversion of $Au_{144}(SCH_2CH_2Ph)_{60}$

Praneeth Reddy Nimmala and Amala Dass*

Department of Chemistry and Biochemistry, University of Mississippi, Oxford, Mississippi 38677, United States

Supporting Information

ABSTRACT: A new aromatic thiolate protected gold nanomolecule $Au_{99}(SPh)_{42}$ has been synthesized by reacting the highly stable $Au_{144}(SCH_2CH_2Ph)_{60}$ with thiophenol, HSPh. The ubiquitous $Au_{144}(SR)_{60}$ is known for its high stability even at elevated temperature and in the presence of excess thiol. This report demonstrates for the first time the reactivity of the $Au_{144}(SCH_2CH_2Ph)_{60}$ with thiophenol to form a different 99-Au atom species. The resulting $Au_{99}(SPh)_{42}$ compound, however, is unreactive and highly stable in the presence of excess aromatic thiol. The molecular formula of the title compound is determined by high resolution electrospray mass spectrometry (ESI-MS) and confirmed by the preparation of the 99-atom nanomolecule using two ligands, namely, $Au_{99}(SPh)_{42}$ and $Au_{99}(SPh\text{-}OMe)_{42}$. This mass spectrometry study is an unprecedented advance in nanoparticle reaction monitoring, in studying the 144-atom to 99-atom size evolution at such high m/z (~12k) and resolution. The optical and electrochemical properties of $Au_{99}(SPh)_{42}$ are reported. Other substituents on the phenyl group, HS-Ph-X, where X = −F, $-CH_3$, $-OCH_3$, also show the Au_{144} to Au_{99} core size conversion, suggesting minimal electronic effects for these substituents. Control experiments were conducted by reacting $Au_{144}(SCH_2CH_2Ph)_{60}$ with HS-$(CH_2)_n$-Ph (where n = 1 and 2), bulky ligands like adamantanethiol and cyclohexanethiol. It was observed that conversion of Au_{144} to Au_{99} occurs only when the phenyl group is directly attached to the thiol, suggesting that the formation of a 99-atom species is largely influenced by aromaticity of the ligand and less so on the bulkiness of the ligand.

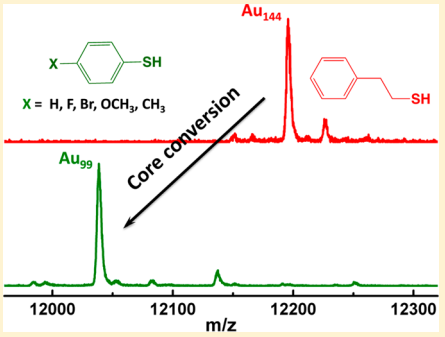

INTRODUCTION

Gold thiolate nanomolecules are ultrasmall gold nanoparticles (<2 nm) of molecular definition and a fixed composition, containing a specific number of gold atoms and capping thiolate ligands.[1−4] Typical examples include $Au_{25}(SR)_{18}$, $Au_{38}(SR)_{24}$, and $Au_{144}(SR)_{60}$. These nanomolecules are stable at ambient conditions, can be dried and redispersed in solvents and can form alloy[4−6] nanomolecules with Ag, Cu and Pd. Gold nanomolecules show size-dependent, optical and electrochemical properties with applications in various fields like catalysis,[7,8] drug delivery[9] and sensing.[10] For using these materials in practical applications, it is crucial to understand the stability under various ligand environments, such as aliphatic ligands, aromatic ligands and bulky ligands.

Research on gold−thiolate nanomolecules over the past two decades predominantly uses aliphatic thiolate ($HS\text{-}C_nH_{2n+1}$) ligands as capping agents. Murray's early work showed that an acetonitrile extract of $Au_m(SCH_2CH_2Ph)_n$ predominantly yielded $Au_{25}(SCH_2CH_2Ph)_{18}$.[12] This acetonitrile solubility of $Au_{25}(SCH_2CH_2Ph)_{18}$ facilitated the isolation of highly pure Au_{25} before size exclusion chromatography (SEC) protocols were established for purification of organo-soluble gold nanomolecules. Subsequently, other larger core sizes such as $Au_{38}(SR)_{24}$, $Au_{144}(SR)_{60}$ were prepared using R=SCH_2CH_2Ph. This was, due in part, to the fact that phenylethanethiol ligated nanomolecules ionize in an efficient manner in MALDI-MS analysis with the DCTB(trans-2-[3[(4-tertbutylphenyl)-2-methyl-2-propenylidene]malononitrile) matrix.[13] Overall, phenylethanethiol has become the most widely used ligand in this field by researchers worldwide. It was found that both aliphatic ligands and phenylethanethiol yield the same core sizes, including 25-, 38-, 67-, 144-metal atom nanomolecules. For the purposes of synthesis of Au-SR nanomolecules, it was found that the chemical differences between aliphatic and phenylethanethiol ligands are only subtle and show minimal variation in the final composition and core-size of the nanomolecules.

In a previous report, we studied the effect of aromaticity on the composition and core-size of Au-SR nanomolecules, using benzenethiol, HSPh.[14] A clear aromaticity effect was observed to form an Au_{36}-atom, instead of Au_{38}-atom nanomolecule. A mixture of Au_{67} and $Au_{\sim 103-105}$ on etching with aliphatic or phenylethanethiol ligands, yields $Au_{38}(SR)_{24}$. On the other hand, the use of benzenethiol yielded $Au_{36}(SPh)_{24}$ core. The initial assignment, $Au_{36}(SPh)_{23}$, solely based on MALDI is now corrected to $Au_{36}(SPh)_{24}$ based on high resolution, isotopically resolved, ESI-MS and X-ray crystal structure.[11] We have shown that $Au_{67}(SCH_2CH_2Ph)_{35}$ and $Au_{\sim 103-105}(SCH_2CH_2Ph)_{\sim 44-46}$[15] convert to $Au_{36}(SPh)_{24}$, via $Au_{38}(SCH_2CH_2Ph)_{14}(SPh)_{10}$ as an intermediate. We noted that when the number of "benzenethiol ligands reaches a

Received: December 1, 2013
Revised: October 7, 2014
Published: November 26, 2014

   dx.doi.org/10.1021/ja5103025 | J. Am. Chem. Soc. 2014, 136, 17016−17023

threshold value", a change in "core size to Au_{36} instead of Au_{38}" occurs.[14] In an independent study, another group recently confirmed this conversion of Au_{38} to Au_{36}, by using $Au_{38}(SCH_2CH_2Ph)_{24}$ as a starting material. This study varied the R group from −H to −*t*-Bu to obtain $Au_{36}(SPh\text{-}tBu)_{24}$ and reported its X-ray crystal structure.[16] A highly important breakthrough in nanomolecules research came in the form of the crystal structure of $Au_{102}(SPh{-}COOH)_{44}$.[17] Though this was the first nanomolecule prepared using an aromatic ligand, it was not reported to study the effect of aromaticity, but the breakthrough focused on X-ray crystallography. Our attempt to prepare $Au_{102}(SCH_2CH_2Ph)_{44}$ or $Au_{102}(SC_nH_{2n+1})_{44}$ has not been successful to date. Instead, we observed that a series of related core sizes $Au_{103}(SR)_{45}$, $Au_{104}(SR)_{45}$, $Au_{104}(SR)_{46}$, and $Au_{105}(SR)_{46}$ were formed when the R group was either $-CH_2CH_2Ph$ or $-SC_6H_{13}$.[15] This could be attributed to the difference in the ligands used for the synthesis. Jin and co-workers showed that $Au_{25}(SCH_2CH_2Ph)_{18}$ nanomolecules on reaction with aromatic ligand converts to $Au_{28}(SPh\text{-}tBu)_{20}$.[18] These results show that aromaticity has a clear effect on the core-size and composition of gold nanomolecules, namely, the core-sizes of aliphatic ligated systems such as Au_{25}, Au_{38}, $Au_{103-105}$ are clearly different than aromatic ligated systems like Au_{28}, Au_{36}, and Au_{102}. An earlier report employed aromatic ligands, HSPh in the direct synthesis to prepare Au:SR clusters with core masses of 5.5, 8.7, 22, and 28 kDa.[19]

While some progress has been made on the effect of aromatic ligands on Au nanomolecules, there is still a lack of understanding on similar effects on the larger core-sized nanomolecules, > 105-gold atoms. Here, we report the effect of aromaticity of the ligands on an ultrastable and larger $Au_{144}(SCH_2CH_2Ph)_{60}$ nanomolecule. MALDI and high resolution ESI mass spectrometry data show that $Au_{144}(SCH_2CH_2Ph)_{60}$ upon reacting with HS-Ph at 80 °C converts to $Au_{99}(SPh)_{42}$. The composition, $Au_{99}(SPh\text{-}X)_{42}$ was confirmed by high resolution ESI-MS using two ligands, −SPh and −SPh-OMe. $Au_{99}(SPh)_{42}$ was characterized using optical spectroscopy, powder X-ray diffraction and differential pulse voltammetry. We studied the core-size conversion using MALDI, ESI-MS and show that after an exchange of 13 ligands, the 144-atom core is unstable and converts to 99-atom core. Data presented for other substituents, where X = −F, and $-CH_3$, also support the formation of Au_{99} core. Furthermore, we studied the effect of linker length between the thiol and phenyl group, by employing HS-Ph, HS-CH_2-Ph and HS-CH_2-CH_2-Ph.[11] We report that only the phenyl group directly attached to thiol groups provides the necessary conjugation for the aromatic effect to manifest and convert the Au_{144} core to Au_{99}, whereas HS-CH_2-Ph and HS-CH_2-CH_2-Ph do not affect the 144-core. Bulky ligands such as adamantanethiol or cyclohexanethiol do not yield an Au_{99} core either.

EXPERIMENTAL SECTION

Chemicals. Phenylethanethiol (Aldrich, ≥ 99%), sodium borohydride (Acros, 99%), *trans*-2-[3-(4-*tert*-butylphenyl)-2-methyl-2-propenylidene]malononitrile (DCTB matrix) (Fluka, ≥ 99%), benzenethiol (Aldrich 97%), 4-methoxybenzenethiol (Aldrich 97%), 4-fluorobenzenethiol (Aldrich 97%), 4- bromobenzenethiol (Aldrich 95%), 5-chloro-2-methyl-benzenethiol and *tert*-butylbenzenethiol (Aldrich 95%) were purchased and used as received. Tetrahydrofuran (anhydrous, stabilized 99.9%) and other solvents like toluene, methanol, acetonitrile and acetone were used from Fisher as received.

Equipment. UV−visible absorption spectra were recorded in toluene on a Shimadzu UV-1601 instrument. Matrix assisted laser desorption time-of-flight (MALDI-TOF) mass spectra were collected on a Bruker Autoflex II mass spectrometer in linear positive mode using a nitrogen laser (337 nm) with DCTB as the matrix.[13] ESI-MS spectra were acquired on Waters SYNAPT mass spectrometer using HPLC grade THF. No additives were used to induce ionization. Electrochemical measurements were performed on a CHI 620 instrument using 5 mg of title compound in DCE solution with 0.5 mM bis(triphenyl phosphoranylidene) ammonium tetrakis (pentafluorophenyl) [$BTPPATBF_{20}$] as supporting electrolyte under nitrogen atmosphere.[20] Powder XRD measurements were performed on Bruker D8-Focus XRD instrument for 48 h on a quartz substrate. 5 mg of sample was dissolved in minimal amount of toluene and deposited on the substrate and air-dried.

Synthesis. The synthesis of Au_{99} involves two steps. The first step is the synthesis of $Au_{144}(SCH_2CH_2Ph)_{60}$ (referred as Au_{144}) using two phase Brust−Schiffrin synthesis[21] followed by etching of Au_{144} with benzenethiol to form $Au_{99}(SPh)_{42}$.

Step 1: Synthesis of Au_{144}. The synthesis of Au_{144} can be done using different protocols reported in the literature.[22−24] Here, for the synthesis of Au_{144}, 0.35 g (0.88 mmol) of $HAuCl_4$ dissolved in 30 mL of distilled water was added to 0.6 g (1.1 mmol) TOABr in 30 mL toluene. The contents were mixed for 30 min at 500 rpm until the gold salt transfers to the organic phase. The organic layer was then transferred into a separate round-bottom flask and 0.45 mL (0.88 × 4 mmol) of phenylethanethiol was added. The reaction mixture was stirred for 60 min at 500 rpm. Then, 0.34g (8.8 mmol) of $NaBH_4$ in 20 mL ice-cold distilled water was added to the reaction mixture instantaneously. Upon addition of $NaBH_4$, the reaction mixture turned dark, indicating the formation of nanoparticles and was stopped after 1 h. The aqueous layer was pipetted out and the contents were dried by rotary evaporation. The resulting product was washed with methanol three times by centrifugal precipitation to remove the excess ligand and dried by rotary evaporation. MALDI-TOF MS analysis of the resulting product showed a mixture of Au_{144} and $Au_{25}(SCH_2CH_2Ph)_{18}$. Au_{25} was separated by successive solvent fractionations using toluene and methanol mixtures, resulting in pure $Au_{144}(SR)_{60}$.

Step 2: Synthesis of Au_{99}. To 10 mg of Au_{144}, 1 mL of benzenethiol was added and the reaction mixture was heated at 80 °C for about 3h.[25] ESI-MS was performed to monitor the progress of the reaction.[26] For complete ligand exchange, a second etching step is sometimes required. Similar protocol was employed for the other substituents of benzenethiol including 4-methoxybenzenethiol, 4-fluorobenzenethiol and 4-methylbenzenethiol. The resulting product was passed through a short SEC column (20 cm with Biorad SX1 beads in stabilized THF)[27] to remove the excess benzenethiol ligand. This avoids the extremely foul thiol smell and the labor required during processing of this product via methanol precipitation in a centrifuge or rotary evaporation. The product which is collected as the eluent is $Au_{99}(SPh)_{42}$ and completely free of benzenethiol.

RESULTS AND DISCUSSION

1. Core-Size Conversion of $Au_{144}(SCH_2CH_2Ph)_{60}$ to $Au_{99}(SPh)_{42}$. $Au_{144}(SCH_2CH_2Ph)_{60}$ is extremely stable at elevated temperature and in the presence of excess aliphatic thiol. When $Au_{144}(SCH_2CH_2Ph)_{60}$ is treated with an aliphatic thiol such as hexanethiol, HSC_6H_{13}, the Au_{144} core is unreactive and unchanged, but all the 60 ligands are exchanged to form, $Au_{144}(SC_6H_{13})_{60}$. Here, we show that $Au_{144}(SCH_2CH_2Ph)_{60}$ upon etching[25] with benzenethiol leads to the formation of $Au_{99}(SPh)_{42}$. Figure 1 shows the MALDI-MS of the aliquots collected from these etching reactions. In the starting material, Au_{144} is the only species observed in mass spectrum, Figure 1 black spectrum. MALDI-MS of a 1 h sample shows no Au_{144}. Instead there are two peaks observed in the mass spectrum at ∼30 kDa and ∼24 kDa mass. The ∼30 kDa peak corresponds to a previously reported $Au_{130}(SPh)_{50}$ and ∼24 kDa peak corresponds to species related to the title compound. With increasing etching time, Au_{99} is the only peak observed in the

dx.doi.org/10.1021/ja5103025 | J. Am. Chem. Soc. 2014, 136, 17016−17023

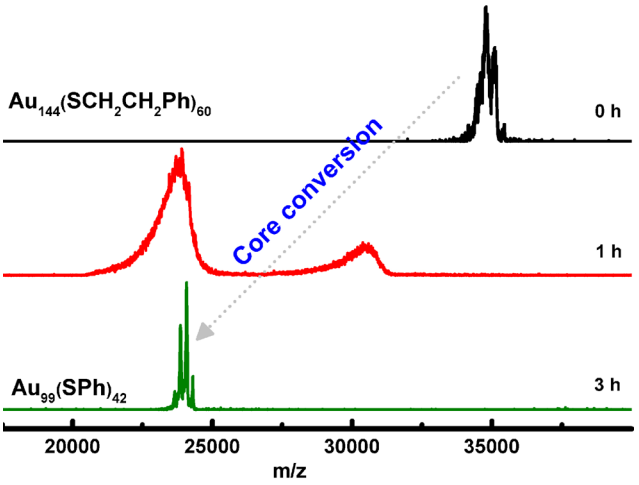

Figure 1. MALDI-MS data of the aliquots collected from the thermochemical treatment of $Au_{144}(SCH_2CH_2Ph)_{60}$ with benzenethiol to obtain the title compound. $Au_{130}(SPh)_{50}$ is seen in the 1 h sample, as an intermediate. The three peaks in the product (olive) corresponds to $Au_{99}(SPh)_{42}$, and other MS fragmentation products, $Au_{99}(SPh)_{40}$ and $Au_{99}(SPh)_{38}$ (see Figure S11).

MALDI-MS data. The $Au_{130}(SPh)_{50}$ peak is present in the 1 h aliquot, but is not observed in the final 3 h product, suggesting its role as an intermediate, vide infra. The mechanism of this reaction is discussed in later sections. The final product obtained from the etching reactions was analyzed by high resolution ESI-MS to determine the composition.

Figure 2a shows the MALDI-MS (red) and ESI-MS (blue) spectra of the final product obtained from the etching reaction. MALDI-MS shows a peak at ~24 kDa, suggesting a singly charged molecular ion. MALDI can lead to fragmentation, especially with labile ligands, so it is essential to use ESI ionization to minimize fragmentation. Nevertheless, a clean MALDI spectrum, without any other lower or higher m/z peaks, indicates the purity of the product. The ionization in ESI-MS occurs in a soft manner resulting in multiply charged, unfragmented molecular ions, typically with higher resolution.[24,28] These multiply charged peaks appear at a lower m/z value, and allow the determination of exact composition. High resolution ESI-MS data (blue curve in Figure 2a) shows peaks at ~12000 and ~8000 m/z, suggesting a charge state of 2+ and 3+ respectively. The experimental 12040 and 8027 m/z peaks match well with that of theoretical values 12041.1 (2+ calc.) and 8026.6 (3+ calc.) corresponding to the composition, $Au_{99}(SPh)_{42}$. We also confirmed the 99:42 Au:ligand mass assignment by preparing the Au_{99} nanomolecules using another ligand. When $Au_{144}(SCH_2CH_2Ph)_{60}$ was etched with *p*-methoxybenzenethiol, HS-Ph-OCH_3, the same core size conversion phenomenon was observed. The final product obtained from the etching of $Au_{144}(SCH_2CH_2Ph)_{60}$ with *p*-methoxybenzenethiol was analyzed by ESI-MS. Figure 2b shows the 3+ peaks observed in ESI-MS for the product obtained with *p*-methoxybenzenethiol (HS-Ph-OCH_3, black spectrum), in comparison with that of benzenethiol (HS-Ph, red spectrum). If both of these peaks correspond to same species with the same metal-atom core, the mass difference between these two peaks should correspond to the difference in the mass of the ligands.[24,29,30] The mass difference between these two peaks was found to be 419 m/z units. Since this is a 3+ ion, the actual mass difference of the molecular ion is 1257

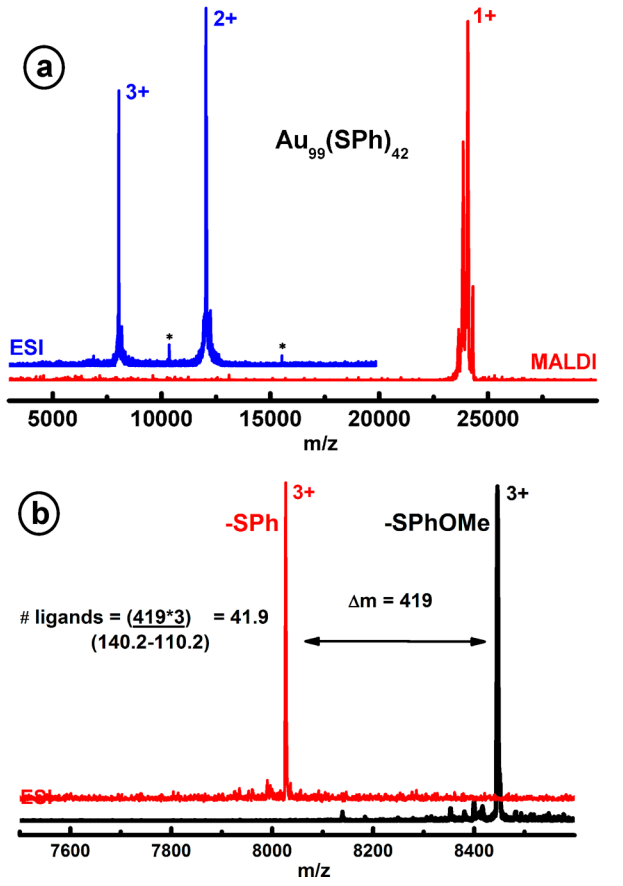

Figure 2. (a) ESI (blue) and MALDI-TOF (red) mass spectrum of $Au_{99}(SPh)_{42}$. The two additional peaks in the MALDI corresponds to MS fragmentation products, $Au_{99}(SPh)_{40}$ and $Au_{99}(SPh)_{38}$. Peaks with asterisks indicate residual $Au_{130}(SPh)_{50}$ intermediate. (b) ESI mass spectra of $Au_{99}(SPh)_{42}$ nanomolecules protected by benzenethiol (red) and *p*-methoxybenezenethiol (black) showing a mass difference of 419 m/z used to calculate the number of ligands to be 42, resulting in the composition, $Au_{99}(SPh)_{42}$.

(3 × 419) Da. When this mass difference is divided by the difference in the mass of the ligands [140.2 (−SPhOCH3) − 110.2 (−SPh) = 30 Da], the number of ligands was found to be 42. This further confirms the 99:42 composition based on the experimental data observed for $Au_{99}(SPh)_{42}$ and $Au_{99}(SPhOCH_3)_{42}$.

2. Characterization of $Au_{99}(SPh)_{42}$. Gold nanomolecules show size-dependent optical and electrochemical properties. Figure 3 shows the UV−vis absorption spectra of $Au_{99}(SPh)_{42}$ measured in toluene in comparison with $Au_{144}(SCH_2CH_2Ph)_{60}$. Though the UV−vis spectra of the nanomolecules in the 70- to 150-atom region lack distinct features, the differences in the spectra of the 99- and 144-atom species are easily observed upon closer inspection. For $Au_{99}(SPh)_{42}$ (olive curve), absorption features at 400 and 600 nm were observed. $Au_{144}(SCH_2CH_2Ph)_{60}$ (red curve) on the other hand, shows features at 520 and 700 nm.

Smaller gold nanomolecules, like Au_{25}, Au_{36}, and Au_{38}, show molecule-like behavior with larger (>1 V) electrochemical gap. As the size of the nanomolecules increases the electrochemical gap decreases and shows bulk metal−type behavior. Between these two extreme behaviors, there is another class of gold nanomolecules termed as quantized double layer (QDL) charging-type by Murray.[31] QDL behavior of nanomolecules

dx.doi.org/10.1021/ja5103025 | J. Am. Chem. Soc. 2014, 136, 17016−17023

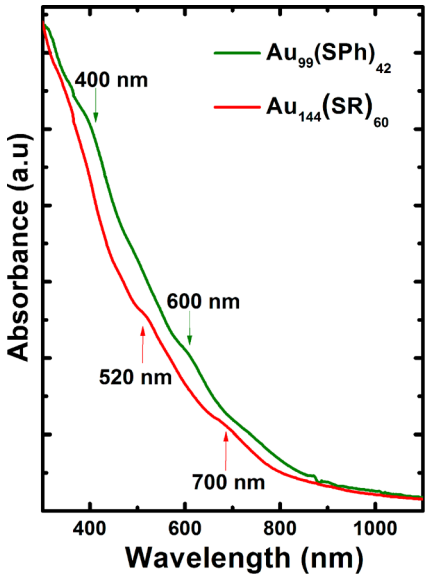

Figure 3. UV−vis absorption spectra of $Au_{99}(SPh)_{42}$ nanomolecules (olive) in toluene in comparison with $Au_{144}(SCH_2CH_2Ph)_{60}$ (red).

is characterized by several redox waves, often with equal potential spacing, observed in the voltammetry experiments. The electrochemical behavior of gold nanomolecules can be studied by cyclic voltammetry (CV) and differential pulse voltammetry (DPV). Figure 4 shows the DPV of Au_{99} in

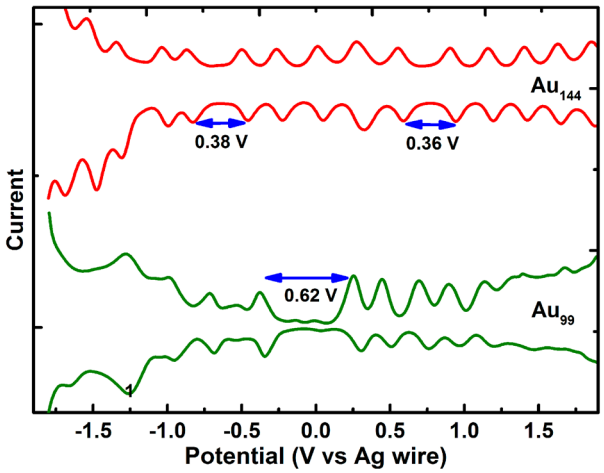

Figure 4. Electrochemistry. Differential pulse voltammetry (DPV) of $Au_{99}(SPh)_{42}$ nanomolecules (olive) measured in 1,2-dichloroethane and 10 mM $BTPPATBF_{20}$ supporting electrolyte. The DPV of $Au_{144}(SCH_2CH_2Ph)_{60}$, red curve, is shown for comparison.

comparison with Au_{144}.[20] The electrochemistry experiments were performed in 1,2-dichloroethane using $BTPPATBF_{20}$ as the supporting electrolyte, reported in literature.[20,32]

The DPV data of Au_{99} shows at least 10 different oxidation and reduction waves. Each of these peaks, correspond to a single electron charging event; meaning an electron is either removed or added to the nanomolecule. The largest potential difference between the two consecutive redox waves, 0.62 V in this case, corresponds to the electrochemical gap. This electrochemical gap is related to the HOMO−LUMO gap in the nanomolecules when accounted for the charging energy imposed to correct for the additional energy required to add or remove an electron. The charging energy can be approximated to the potential difference between the first and second oxidation peaks,[33] which is 0.2 V in this case. Thus, the HOMO−LUMO gap, after correcting for the charging energy from electrochemical gap, was found to be about 0.4 eV. This corrected electrochemical gap falls in-line with the trend of the reported values for other molecule-like species like, Au_{25}, Au_{38}, Au_{67} and Au_{144} (1.6 V, 1.2 V, 0.74 and 0.3 V respectively)[20,29,34−36] and agrees with the molecule-like to bulk-metal type transition expected for gold nanomolecules. The redox behavior of Au_{99} is clearly different than that of $Au_{144}(SCH_2CH_2Ph)_{60}$. Au_{144} has 15 redox waves in the potential window under consideration (see Figure 4, red curve). There are three potential spacings of ∼350 mV, centered at +0.7, −0.6, and −1.1 V. The approximate spacing of the other redox waves is ∼250 mV. Note that our Au_{144} DPV behavior is slightly different than that of the literature reports, and this could be due to the differences in the purity of the samples used for the reports published in early 2000s.[20,31,37,38] Many attempts were made to improve the consistency of the forward and return sweeps of Au_{99} DPV. We could not attain identical redox behavior in forward and return sweeps, but this is beyond the scope of this report on Au_{99} and warrants a full detailed electrochemical study. Au_{99} exhibits several oxidation and reduction peaks in the DPV experiments with a smaller electrochemical gap. The behavior is in the transition region between molecule-like to QDL behavior, possessing some characteristics of both. Nevertheless, the core conversion of Au_{144} to Au_{99} manisfests itself in their corresponding electrochemical behaviors in two ways: (a) a larger electrochemical gap is observed for Au_{99} when compared with the larger Au_{144} as expected; (b) the fingerprint observed in the electrochemical redox waves are unique for Au_{144} versus Au_{99}, offering further support for the 144 to 99-Au atom core size conversion.

To study the atomic structure of $Au_{99}(SPh)_{42}$, powder X-ray diffraction (XRD) of the nanomolecule was measured. Figure 5 shows the powder XRD of Au_{99} (olive) in comparison with Au_{144} (red), Au_{67} (black), Au_{36} (brown) and the theoretical face centered cubic (*fcc*) pattern for bulk-like Au (blue). The powder X-ray diffraction pattern of the title compound is distinct. $Au_{67}(SR)_{35}$ is proposed to have a Marks-decahedral structure.[29,39] A peak corresponding to the (200) fcc bulk structure is observed as a shoulder in the powder XRD spectra of Au_{36}. The Au_{99} however does not have this shoulder, and therefore is not likely to have an fcc structure. On the basis of the powder XRD data alone, it is not possible to determine if the atomic structure has changed from the Au_{144} to Au_{99}. Further experiments including single crystal X-ray diffraction data are needed to elucidate the structure and bonding of $Au_{99}(SPh)_{42}$ nanomolecules. It would be interesting to check if the structure of $Au_{99}(SPh)_{42}$ is related to the crystallographically determined structure of $Au_{102}(SPhCOOH)_{44}$; however, attempts to grow single crystals have not yielded X-ray quality crystals to date.[16,42] If the structure has only the monomeric [-SR-Au-SR-] units, then it would lead to a Au_{78} + 21[-SR-Au-SR-] structure. The 78-atom core cannot be easily attained from the Au_{49} atom core shown in the Kornberg's study. On the basis of this argument alone, it is possible that the 99-atom structure is vastly different than that of the 102-metal atom core. The properties of $Au_{99}(SPh)_{42}$ are summarized in Table 1.

dx.doi.org/10.1021/ja5103025 | J. Am. Chem. Soc. 2014, 136, 17016−17023

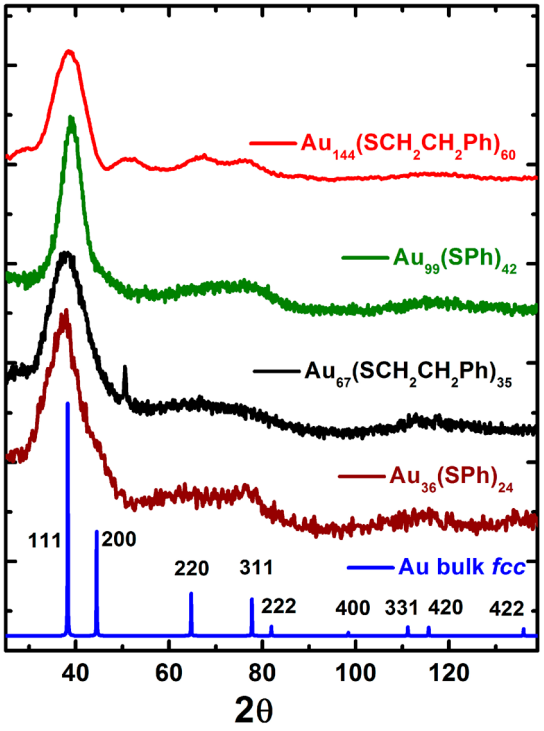

Figure 5. Powder X-ray diffraction pattern of $Au_{99}(SPh)_{42}$ nanomolecules (olive) in comparison with that of $Au_{144}(SCH_2CH_2Ph)_{60}$ (red), $Au_{67}(SCH_2CH_2Ph)_{35}$ (black), $Au_{36}(SPh)_{24}$ (red), and the pattern for bulk-like *fcc* Au(blue).

Table 1. Properties of $Au_{99}(SPh)_{42}$ Nanomolecules

Molecular weight	24079.4 (expt.), 24082.2 (calc.)
Color	brown
Optical features	features at 400 and 600 nm
Solubility	highly soluble in THF and CH_2Cl_2 (>20 mg/mL) and sparingly soluble in toluene (~5 mg/mL)
Stability	air, moisture, 80 °C in toluene or PhSH
Atomic structure	non-fcc powder XRD patterns
Redox properties	ten redox waves, electrochemical gap of 0.62 V
$Au_{144} \rightarrow Au_{99}$ conversion details	Up to $Au_{144}(SPh)_{13}(SCH_2CH_2Ph)_{47}$ is stable. When the HSPh exchange exceeds 13, the 144-atom core converts to $Au_{99}(SPh)_{42}$

3. $Au_{144} \rightarrow Au_{99}$ Core-Size Conversion Studied by ESI-MS: A Case of Ligand Aromaticity Instead of Ligand Bulkiness. To study the Au_{99} formation, we have followed the ligand exchange reaction[40] of Au_{144} with ESI mass spectrometry.[41−44] ESI-MS produces multiply charged species, which appear at a lower mass and offer better resolution, enabling us to identify the exchanges on Au_{144}. The peak at 12198 m/z is for the starting material (3+ of Au_{144}). Note that the molecular weight of phenylethanethiolate and benzenethiolates correspond to 137.2 and 109.2 Da, respectively. In 10 min, there is an envelope of peaks at lower mass, corresponding to the 3+ ions of $Au_{144}(SCH_2CH_2Ph)_{60-n}(SPh)_n$, where the $n_{average}$ is 5 and $n_{maximum}$ is ~13 benzenethiolates. All the species seem to still remain as 144-Au atom species. In 20 min, there are two distinct envelopes of peaks: (a) one corresponding to $Au_{144}(SCH_2CH_2Ph)_{60-x}(SPh)_x$, where x has increased to 9; (b) a second peak emerging at ~12039 m/z corresponding to the 2+ of $Au_{99}(SPh)_{42-m}(SCH_2CH_2Ph)_m$. In 30 min sample, the reaction is near completion, where the 99-Au atom species dominates and the 144-atom species is present as a minor (~10%) fraction. The 40 min sample contains the fully exchanged, $Au_{99}(SPh)_{42}$ in addition to minor amounts of $Au_{99}(SPh)_{42-m}(SCH_2CH_2Ph)_m$, where m = 1 and 2. The last one or two (m =1 or 2) ligand exchanges do not reach completion to m = 0, as an equilibration state is reached due to the $-SCH_2CH_2Ph$ ligands released during the ligand exchange. Typically, a second etching process, denoted as "re-etch" in the figure, is conducted, where the product of first etching is washed and reacted with a fresh addition of benzenethiol for 30 min at 80 °C. This is necessary to drive the reaction to completion to form $Au_{99}(SPh)_{42}$, shown in the "re-etch" spectra in Figure 6. The same observation was made in case of

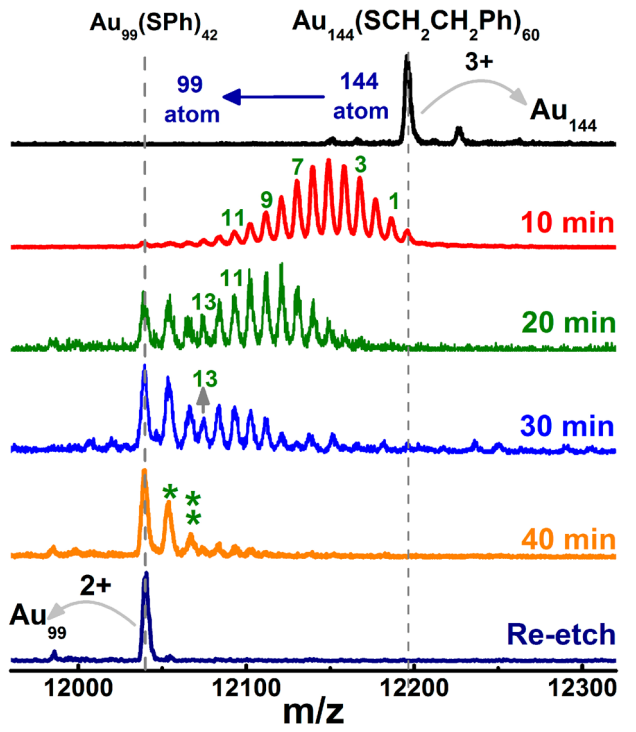

Figure 6. ESI-MS monitoring of the thermo-chemical treatment of $Au_{144}(SCH_2CH_2Ph)_{60}$ in benzenethiol. The spectra are expanded in the 12 kDa mass region to highlight the ligand exchanges occurring in the early stage of reaction. Note that when n in $Au_{144}(SCH_2CH_2Ph)_{60-n}(SPh)_n$ excess a value of 13, it converts to the Au_{99} core Further exchanges lead to formation of $Au_{99}(SPh)_{42}$ (2+ at 12,039 m/z). $Au_{99}(SPh)_{41}(SCH_2CH_2Ph)_1$ and $Au_{99}(SPh)_{40}(SCH_2CH_2Ph)_2$ species are denoted by olive asterisks. Note that in this plot, Au_{144} is a 3+ ion and the Au_{99} is a 2+ ion as indicated by the mass differences in ligand exchange products to be 9.3 and 14 m/z, respectively.

synthesis of Au_{36}[14] where a second etching was needed for complete exchange by benzenethiol. Careful observation shows that after ~13 ligand exchanges, the Au_{144} core becomes unstable and converts to an entirely different core, Au_{99}. That is, as the value of n in $Au_{144}(SCH_2CH_2Ph)_{60-n}(SPh)_n$ becomes larger than 13, the effect induced by the aromatic ligands reaches a threshold value, at which point the Au_{144} core starts converting to Au_{99} core. We hypothesize that the core size conversion after 13 ligands is a consequence of the aromaticity associated with the benzenethiolate ligands. That is introducing 13 or more aromatic ligands, which are known to have

dx.doi.org/10.1021/ja5103025 | J. Am. Chem. Soc. 2014, 136, 17016−17023

secondary stabilizing interactions, are likely promoting the conversion of Au_{144} to Au_{99}. In a separate set of experiments, we have performed etching of $Au_{144}(SCH_2CH_2Ph)_{60}$ in sterically bulky ligands like cyclohexanethiol and adamantanethiol. The results (not shown here) indicate the formation of a number of lower clusters (<10000 Da) without any $Au_{99}(SR)_{42}$ signatures, and is beyond the scope of this work. These results from bulky ligand etching show that (a) $Au_{99}(SPh)_{42}$ is only formed when aromatic thiolate ligands are used; (b) supports the hypothesis that $Au_{144} \rightarrow Au_{99}$ conversion is strongly dictated by the *aromaticity* of the ligands; (c) bulkiness may play a role, but bulkiness alone does not lead to the formation of Au_{99}. The mass spectrometry study shown in Figure 6 is a first time report of nanoparticle reaction monitoring at high mass, high resolution, used in studying the size evolution of such a large nanomolecule (>100 atoms).

In addition to etching of Au_{144} in aromatic ligands, we have investigated the etching of higher clusters[45] (between 50 and 150 kDa). This mixture of higher clusters also undergoes a core conversion to yield Au_{99} in 3 h (see Figure S3). To ensure that the Au_{99} in this reaction is coming from the higher clusters and not the Au_{144}, we have separated the former (only cluster > Au_{144}) using size exclusion chromatography.[27] Finally, a mixture of Au_{144} and clusters > Au_{144} when etched in benzenethiol also gave Au_{99} as the only final product. These results combined with the reports on Au_{36} show that Au_{99} and Au_{36} are core-sizes stabilized by aromatic ligands under etching. Au_{36} is stable in lower mass regions, and Au_{99} is stable in higher mass regions. Here we note that $Au_{102}(SPh{-}COOH)_{44}$[17] is water-soluble and the $Au_{99}(SPh)_{42}$ is organic soluble. Since the mass spectrometry of water-soluble nanomolecules, and in particular larger ones, is not well established, lack of further experiments using the 4-carboxybenzenethiol.

4. Substituent Effects on the Core Conversion of $Au_{144} \rightarrow Au_{99}$. We have performed the ligand exchange of Au_{144} with substituted benzenethiols of the form HS-Ph-X, to study the effect of the substituent on the Au_{144} to Au_{99} reaction.[46] In this study, we have used 4-methoxybenzenethiol, 4-fluorobenzenethiol and 4-methylbenzenethiol in addition to benzenethiol. All the four ligands have shown core conversion of Au_{144} to Au_{99}. 4-methoxybenzenethiol has produced $Au_{99}(SPh\text{-}OMe)_{42}$ which was analyzed both by ESI-MS and MALDI-MS. The end products of reactions using 4-fluorobenzenethiol and 4-methylbenzenethiol were analyzed by MALDI-MS only (Figure 7), since ESI-MS showed no signal for these samples. Although the exact assignments could not be made using these two ligands, the experimentally observed masses are close to the predicted mass for $Au_{99}(SPh\text{-}F)_{42}$ (calc. 24 667 Da) and $Au_{99}(SPh{-}CH_3)_{42}$ (calc. 24 834 Da). We did not attempt to assign the composition for these two products due to the low resolution of MALDI-MS at this mass range. For the ligands considered here, the 144 → 99 core-size conversion is due to the aromaticity of the ligand; with the electronic effects due to substituents' on the aromatic ring, imposing only minimal influence.

5. Effect of Conjugation of Ligands on the 144 → 99 Core Conversion. The effect of linker length between the benzene ring and thiol group on the $Au_{144} \rightarrow Au_{99}$ core size conversion was investigated. The thermochemical stability of Au_{144} is known for nearly two decades now.[1,23−25,47] $Au_{144-x}Ag_x(SR)_{60}$ is also prepared by silver doping, suggesting the high stability of the 144-atom species.[6] When $Au_{144}(SCH_2CH_2Ph)_{60}$ was etched in phenylethanethiol at 80 °C, it is stable and remains as 144-atom core for over 24 h (Figure 8, black spectrum). Etching of $Au_{144}(SC_nH_{2n+1})_{60}$ in HS-CH_2-CH_2-Ph also yields $Au_{144}(SCH_2CH_2Ph)_{60}$ without affecting the 144-atom core. In this study, we have etched $Au_{144}(SCH_2CH_2Ph)_{60}$ with HS-CH_2-CH_2-Ph, HS-CH_2-Ph, and HS-Ph. In other words, the effect of linker length, n in HS-$(CH_2)_n$-Ph was varied by one methylene group each from n = 2, 1, and 0. We observed that both HS-CH_2-CH_2-Ph and HS-CH_2-Ph maintains the 144-core and do not convert it to 99. This is shown in the black and olive MALDI spectra in Figure 8. However, when −Ph is directly connected to the thiol group, it converts to Au_{99}, as shown in red curve in Figure 8. It is clear from these results that a direct conjugation of benzene ring with thiol group is necessary for the $Au_{144} \rightarrow Au_{99}$ conversion.

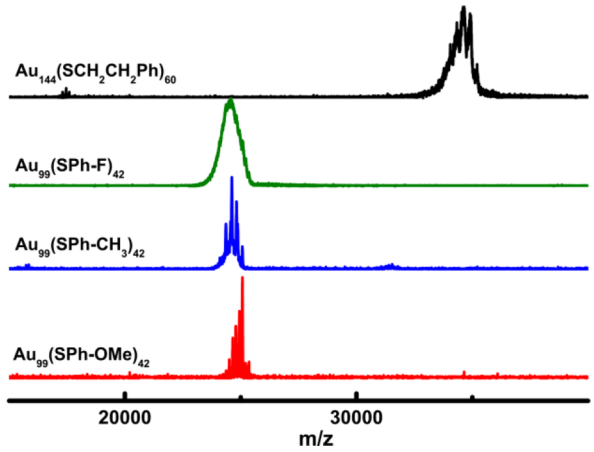

Figure 7. MALDI-MS of the products obtained by core conversion of $Au_{144}(SCH_2CH_2Ph)_{60}$ using various substituents of benzenethiol including 4-fluorobenzenethiol, 4-methylbenzenethiol and 4-methoxybenzenethiol.

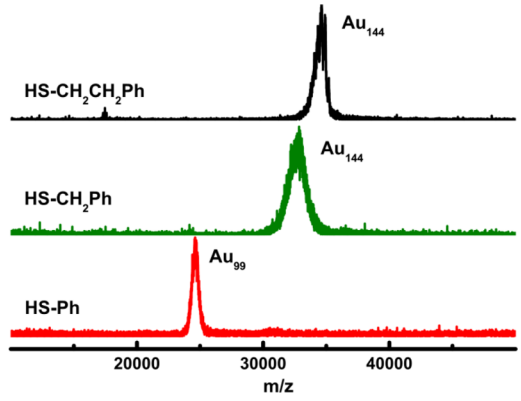

Figure 8. MALDI-MS of products obtained by etching $Au_{144}(SCH_2CH_2Ph)_{60}$ in $PhCH_2CH_2SH$ (black), $PhCH_2SH$ (olive) and PhSH (red).

6. Mechanism and Yield of Core Size Conversion to $Au_{99}(SPh)_{42}$. The mechanism of the core size conversion of Au_{144} to Au_{99} is not clear. Whether the downsizing process occurs by either a) the loss of ligands and gold atoms from the surface of gold nanomolecules or b) some form of structural rearrangement of the core, where the new core sizes are formed from either larger or smaller gold nanomolecules, is not clear. In our earlier report on $Au_{36}(SPh)_{24}$, there is an intermediate observed with the composition $Au_{38}(SPh)_{\sim 10}(SCH_2CH_2Ph)_{\sim 14}$.

dx.doi.org/10.1021/ja5103025 | J. Am. Chem. Soc. 2014, 136, 17016−17023

This was also confirmed in the core size conversion of $Au_{38}(SCH_2CH_2Ph)_{24}$ to $Au_{36}(SPh\text{-}tBu)_{24}$. The 30 kDa peak observed in the 1 h MALDI spectrum of Figure 1 is for $Au_{130}(SPh)_{50}$, which may be an intermediate in this reaction. In our recent report, we have shown that $Au_{130}(SR)_{50}$ is a stable core size which is formed when larger (>40 kDa) clusters are etched with thiols. The 130,50 composition had been demonstrated using three different ligands ($-SCH_2CH_2Ph$, $-SC_6H_{13}$, $-SC_{12}H_{25}$) and as alloys ($Au_{130-x}Ag_x(SR)_{50}$, $Au_{130-x}Pd_x(SR)_{50}$).[48] But in this reaction, it is an intermediate formed in the reaction but is less stable compared to the final product Au_{99}. Etching the higher mass nanomolecules capped by phenylethanethiol in thiophenol yields Au_{99} and not Au_{130} (see Figure S3). Typically, 10 mg $Au_{144}(SCH_2CH_2Ph)_{60}$ yields ~3 mg of $Au_{99}(SPh)_{42}$ with considerable insoluble material in the reaction flasks that could be attributed to Au-SR polymers as identified before.

7. Instability of $Au_{144}(SR)_{60}$, (R = Aliphatic) Upon Reaction with Aromatic Thiols. $Au_{144}(SR)_{60}$ is considered one of the most ubiquitous and robust core size, and is shown to be highly stable with phenylethanethiol ligand upon rigorous etching.[24,49−51] Au−Ag,[52] Au−Pd,[53] Au−Cu,[54] alloy nanomolecules of Au_{144} such as $Au_{144-x}Ag_x(SCH_2CH_2Ph)_{60}$, $Au_{144-x}Ag_x(SCH_2CH_2Ph)_{60}$, $Au_{144-x}Cu_x(SCH_2CH_2Ph)_{60}$ have been prepared and shown to be stable. On the basis of NMR spectroscopy, Au_{144} protected with para-mercaptobenzoic acid (pMBA) ligands were found to be symmetric.[55] The same research group subsequently showed that pMBA protected Au_{144} is not a cluster that results from synthesis in excess pMBA,[56] consistent with our findings. However, the assignment in this NMR study was made from low resolution mass spectrometry data and needs further investigation. The results presented in this work clearly show that $Au_{144}(SR)_{60}$ is unstable when reacted with aromatic thiols, HS-Ph-X, where X = −H, $-OCH_3$, −F and $-CH_3$. High resolution mass spectrometry of the putative $Au_{144}(S\text{-}pMBA)_{60}$ and more systematic studies from independent research groups will shed more light on these issues.

CONCLUSION

In summary, we report the synthesis, purification and characterization of an all aromatic, $Au_{99}(SPh)_{42}$ nanomolecule. We have assigned its molecular formula using ESI-MS, characterized it using UV−vis−NIR, powder-XRD and voltammetry. This study sheds light on the instability of Au_{144} upon reaction with aromatic ligands. The results show that the aromaticity effects alter the stability in different ways, yields cores that are different than aliphatic protected ligands. Since there appears to be no preferred charge state, there is no indication of any special stability associated with the electron shell closing for the $Au_{99}(SPh)_{42}$ composition. We hope the methodologies used in this report to synthesize all-aromatic nanomolecles will spur further experimental research. Future research directions include the comparing the properties of Au_{99} with that of $Au_{102}(SPh{-}COOH)_{44}$[17] as they are closely related to Au_{99} in size. This is currently hindered due to difficulties in purification and mass spectrometric characterization of water-soluble nanomolecules. Theoretical structure modeling,[3,57−62] chemical analysis[63] and electronic structure calculations[64] will facilitate the understanding of the title compound reported here.[65]

ASSOCIATED CONTENT

Supporting Information

Detailed synthetic conditions, additional mass spectra, and reproducibility data. This material is available free of charge via the Internet at http://pubs.acs.org.

AUTHOR INFORMATION

Corresponding Author

amal@olemiss.edu

Notes

The authors declare no competing financial interest.

ACKNOWLEDGMENTS

NSF-CHE-1255519 supported the work performed. We thank Jared Delcamp and Vijay Reddy Jupally for discussions.

REFERENCES

(1) Whetten, R. L.; Khoury, J. T.; Alvarez, M. M.; Murthy, S.; Vezmar, I.; Wang, Z. L.; Stephens, P. W.; Cleveland, C. L.; Luedtke, W. D.; Landman, U. *Adv. Mater.* **1996**, *8*, 428.
(2) Maity, P.; Xie, S.; Yamauchi, M.; Tsukuda, T. *Nanoscale* **2012**, *4*, 4027.
(3) Pei, Y.; Zeng, X. C. *Nanoscale* **2012**, *4*, 4054.
(4) Negishi, Y.; Kurashige, W.; Niihori, Y.; Nobusada, K. *Phys. Chem. Chem. Phys.* **2013**, *15*, 18736.
(5) Fields-Zinna, C. A.; Crowe, M. C.; Dass, A.; Weaver, J. E. F.; Murray, R. W. *Langmuir* **2009**, *25*, 7704.
(6) Kumara, C.; Dass, A. *Nanoscale* **2012**, *4*, 4084−4086.
(7) Chen, W.; Chen, S. *Angew. Chem., Int. Ed.* **2009**, *48*, 4386.
(8) Tsunoyama, H.; Ichikuni, N.; Sakurai, H.; Tsukuda, T. *J. Am. Chem. Soc.* **2009**, *131*, 7086.
(9) Bowman, M.-C.; Ballard, T. E.; Ackerson, C. J.; Feldheim, D. L.; Margolis, D. M.; Melander, C. *J. Am. Chem. Soc.* **2008**, *130*, 6896.
(10) Lin, C.-A. J.; Yang, T.-Y.; Lee, C.-H.; Huang, S. H.; Sperling, R. A.; Zanella, M.; Li, J. K.; Shen, J.-L.; Wang, H.-H.; Yeh, H.-I.; Parak, W. J.; Chang, W. H. *ACS Nano* **2009**, *3*, 395.
(11) Nimmalla, P. R.; Knoppe, S.; Jupally, V. R.; Delcamp, J. H.; Aikens, C. M.; Dass, A. *J. Phys. Chem. B.* **2014**, DOI: 10.1021/jp506508x.
(12) Donkers, R. L.; Lee, D.; Murray, R. W. *Langmuir* **2004**, *20*, 1945.
(13) Dass, A.; Stevenson, A.; Dubay, G. R.; Tracy, J. B.; Murray, R. W. *J. Am. Chem. Soc.* **2008**, *130*, 5940.
(14) Nimmala, P. R.; Dass, A. *J. Am. Chem. Soc.* **2011**, *133*, 9175.
(15) Dass, A.; Nimmala, P. R.; Jupally, V. R.; Kothalawala, N. *Nanoscale* **2013**, *135*, 10011.
(16) Zeng, C.; Qian, H.; Li, T.; Li, G.; Rosi, N. L.; Yoon, B.; Barnett, R. N.; Whetten, R. L.; Landman, U.; Jin, R. *Angew. Chem., Int. Ed.* **2012**, *51*, 13114.
(17) Jadzinsky, P. D.; Calero, G.; Ackerson, C. J.; Bushnell, D. A.; Kornberg, R. D. *Science* **2007**, *318*, 430.
(18) Zeng, C.; Li, T.; Das, A.; Rosi, N. L.; Jin, R. *J. Am. Chem. Soc.* **2013**, *135*, 10011.
(19) Price, R. C.; Whetten, R. L. *J. Am. Chem. Soc.* **2005**, *127*, 13750.
(20) Quinn, B. M.; Liljeroth, P.; Ruiz, V.; Laaksonen, T.; Kontturi, K. s. *J. Am. Chem. Soc.* **2003**, *125*, 6644.
(21) Brust, M.; Walker, M.; Bethell, D.; Schiffrin, D. J.; Whyman, R. *J. Chem. Soc., Chem. Commun.* **1994**, 801.
(22) Alvarez, M. M.; Khoury, J. T.; Schaaff, T. G.; Shafigullin, M.; Vezmar, I.; Whetten, R. L. *Chem. Phys. Lett.* **1997**, *266*, 91.
(23) Ingram, R. S.; Hostetler, M. J.; Murray, R. W.; Schaaff, T. G.; Khoury, J. T.; Whetten, R. L.; Bigioni, T. P.; Guthrie, D. K.; First, P. N. *J. Am. Chem. Soc.* **1997**, *119*, 9279.
(24) Chaki, N. K.; Negishi, Y.; Tsunoyama, H.; Shichibu, Y.; Tsukuda, T. *J. Am. Chem. Soc.* **2008**, *130*, 8608.
(25) Schaaff, T. G.; Whetten, R. L. *J. Phys. Chem. B* **1999**, *103*, 9394.

(26) Dharmaratne, A. C.; Krick, T.; Dass, A. *J. Am. Chem. Soc.* **2009**, *131*, 13604.
(27) Knoppe, S.; Boudon, J.; Dolamic, I.; Dass, A.; Burgi, T. *Anal. Chem.* **2011**, *83*, 5056.
(28) Tracy, J. B.; Kalyuzhny, G.; Crowe, M. C.; Balasubramanian, R.; Choi, J.-P.; Murray, R. W. *J. Am. Chem. Soc.* **2007**, *129*, 6706.
(29) Nimmala, P. R.; Yoon, B.; Whetten, R. L.; Landman, U.; Dass, A. *J. Phys. Chem. A* **2013**, *117*, 504.
(30) There is literature precedence for this approach, as there are many nanoparticles including $Au_{25}(SR)_{18}$, $Au_{38}(SR)_{24}$, $Au_{67}(SR)_{35}$, $Au_{144}(SR)_{60}$ reported in literature with two or more closely related ligands to yield the same composition.
(31) Heaven, M. W.; Dass, A.; White, P. S.; Holt, K. M.; Murray, R. W. *J. Am. Chem. Soc.* **2008**, *130*, 3754.
(32) The reason for choosing this supporting electrolyte over other commercially available electrolyte salts is the larger potential window offered by $BTPPATBF_{20}$.
(33) Chen, S.; Murray, R. W.; Feldberg, S. W. *J. Phys. Chem. B* **1998**, *102*, 9898.
(34) Lee, D.; Donkers, R. L.; Wang, G.; Harper, A. S.; Murray, R. W. *J. Am. Chem. Soc.* **2004**, *126*, 6193.
(35) Toikkanen, O.; Ruiz, V.; Ronnholm, G.; Kalkkinen, N.; Liljeroth, P.; Quinn, B. M. *J. Am. Chem. Soc.* **2008**, *130*, 11049.
(36) Koivisto, J.; Malola, S.; Kumara, C.; Dass, A.; Hakkinen, H.; Pettersson, M. *J. Phys. Chem. Lett.* **2012**, *3*, 3076.
(37) Hicks, J. F.; Miles, D. T.; Murray, R. W. *J. Am. Chem. Soc.* **2002**, *124*, 13322.
(38) Miles, D. T.; Leopold, M. C.; Hicks, J. F.; Murray, R. W. *J. Electroanal. Chem.* **2003**, *87*, 554.
(39) Whetten, R. L.; Shafigullin, M. N.; Khoury, J. T.; Schaaff, T. G.; Vezmar, I.; Alvarez, M. M.; Wilkinson, A. *Acc. Chem. Res.* **1999**, *32*, 397.
(40) Heinecke, C. L.; Ni, T. W.; Malola, S.; Makinen, V.; Wong, O. A.; Hakkinen, H.; Ackerson, C. J. *J. Am. Chem. Soc.* **2012**, *134*, 13316.
(41) Dass, A.; Holt, K.; Parker, J. F.; Feldberg, S. W.; Murray, R. W. *J. Phys. Chem. C* **2008**, *112*, 20276.
(42) Jupally, V. R.; Kota, R.; Dornshuld, E. V.; Mattern, D. L.; Tschumper, G. S.; Jiang, D.-e.; Dass, A. *J. Am. Chem. Soc.* **2011**, *133*, 20258.
(43) Niihori, Y.; Matsuzaki, M.; Pradeep, T.; Negishi, Y. *J. Am. Chem. Soc.* **2013**, *135*, 4946.
(44) Zeng, C.; Liu, C.; Pei, Y.; Jin, R. *ACS Nano* **2013**, *7*, 6138.
(45) Dass, A. *J. Am. Chem. Soc.* **2011**, *133*, 19259.
(46) Guo, R.; Murray, R. W. *J. Am. Chem. Soc.* **2005**, *127*, 12140.
(47) Schaaff, T. G.; Shafigullin, M. N.; Khoury, J. T.; Vezmar, I.; Whetten, R. L. *J. Phys. Chem. B* **2001**, *105*, 8785.
(48) Jupally, V. R.; Dass, A. *Phys. Chem. Chem. Phys.* **2014**, *16*, 10473.
(49) Bahena, D.; Bhattarai, N.; Santiago, U.; Tlahuice, A.; Ponce, A.; Bach, S. B. H.; Yoon, B.; Whetten, R. L.; Landman, U.; Jose-Yacaman, M. *J. Phys. Chem. Lett.* **2013**, *4*, 975.
(50) Weissker, H. C.; Escobar, H. B.; Thanthirige, V. D.; Kwak, K.; Lee, D.; Ramakrishna, G.; Whetten, R. L.; Lopez-Lozano, X. *Nat. Commun.* **2014**, *5*, 3785.
(51) Schaaff, T. G.; Shafigullin, M. N.; Khoury, J. T.; Vezmar, I.; Whetten, R. L. *J. Phys. Chem. B* **2001**, *105*, 8785.
(52) Kumara, C.; Dass, A. *Nanoscale* **2011**, *3*, 3064.
(53) Kothalawala, N.; Kumara, C.; Ferrando, R.; Dass, A. *Chem. Commun.* **2013**, *49*, 10850.
(54) Dharmaratne, A. C.; Dass, A. *Chem. Commun.* **2014**, *50*, 1722.
(55) Tvedte, L. M.; Ackerson, C. J. *J. Phys. Chem. A* **2014**, *118*, 8124.
(56) Wong, O. A.; Heinecke, C. L.; Simone, A. R.; Whetten, R. L.; Ackerson, C. J. *Nanoscale* **2012**, *4*, 4099.
(57) Gao, Y.; Shao, N.; Zeng, X. C. *ACS Nano* **2008**, *2*, 1497.
(58) Han, Y.-K.; Kim, H.; Jung, J.; Choi, Y. C. *J. Phys. Chem. C* **2010**, *114*, 7548.
(59) Walter, M.; Akola, J.; Lopez-Acevedo, O.; Jadzinsky, P. D.; Calero, G.; Ackerson, C. J.; Whetten, R. L.; Gronbeck, H.; Häkkinen, H. *Proc. Natl. Acad. Sci. U. S. A.* **2008**, *105*, 9157.
(60) Aikens, C. M. *J. Phys. Chem. Lett.* **2010**, *2*, 99.
(61) Jiang, D.-e. *Nanoscale* **2013**, *5*, 7149.
(62) Häkkinen, H. *Nat. Chem.* **2012**, *4*, 443.
(63) Reimers, J. R.; Wang, Y.; Cankurtaran, B. O.; Ford, M. J. *J. Am. Chem. Soc.* **2010**, *132*, 8378.
(64) Hulkko, E.; Lopez-Acevedo, O.; Koivisto, J.; Levi-Kalisman, Y.; Kornberg, R. D.; Pettersson, M.; Häkkinen, H. *J. Am. Chem. Soc.* **2011**, *133*, 3752.
(65) During the revision of this manuscript, another closely related work has been published: Li, G.; Zeng, C.; Jin, R. *J. Am. Chem. Soc.* **2014**, *136*, 3673.